DMD Fast Forward. Published on November 4, 2020 as DOI: 10.1124/dmd.120.000161
This article has not been copyedited and formatted. The final version may differ from this version.

1. Title Page

Title:

Extension of the mechanistic tissue distribution model of Rodgers & Rowland by systematic incorporation of lysosomal trapping: impact on Kpu and volume of distribution predictions in the rat

Authors:

- Maximilian V. Schmitt
- Andreas Reichel
- Xiaohui Liu
- Gert Fricker
- Philip Lienau

Primary laboratory of origin:

Bayer AG
Müllerstraße 178
13353 Berlin, Germany

Affiliations:

- Bayer AG, Pharmaceuticals R&D, Translational Sciences, Research Pharmacokinetics (MVS, PL, AR)
- School of Life Sciences, Tsinghua University, China (XL)
- Institute of Pharmacy and Molecular Biotechnology, University of Heidelberg, Germany. (MVS, GF)

DMD Fast Forward. Published on November 4, 2020 as DOI: 10.1124/dmd.120.000161
This article has not been copyedited and formatted. The final version may differ from this version.

2. Running Title Page

Running Title:

Drug tissue distribution incorporating lysosomal trapping

Corresponding author:

Name: Dr. Philip Lienau

Address: Bayer AG
Building S116, 550
13342 Berlin, Germany

Tel: +49 30 468-18507

E-Mail: philip.lienau@bayer.com

File information:

- Number of text pages: 20
- Number of tables: 5
- Number of figures: 6
- Number of references: 44
- Number of words in the Abstract: 247
- Number of words in the Introduction: 713
- Number of words in the Discussion: 1492

DMD Fast Forward. Published on November 4, 2020 as DOI: 10.1124/dmd.120.000161
This article has not been copyedited and formatted. The final version may differ from this version.

List of nonstandard abbreviations:

BMP - bis(monoacylglycero)phosphate

Kp – partition coefficient

Kpu – unbound partition coefficient

PKI – protein kinase inhibitor

Vss – volume of distribution at steady state

Vuss – unbound volume of distribution at steady state

DMD Fast Forward. Published on November 4, 2020 as DOI: 10.1124/dmd.120.000161
This article has not been copyedited and formatted. The final version may differ from this version.

3. Abstract

Physiologically based pharmacokinetic (PBPK) modelling has become a standard tool to predict drug distribution in early stages of drug discovery which however currently does not encompass lysosomal trapping. For basic-lipophilic compounds lysosomal sequestration is known to potentially influence intracellular as well as tissue distribution. The aim of our research was to reliably predict the lysosomal drug content and ultimately integrate this mechanism into PK prediction models. First, we further validated our previously presented method to predict the lysosomal drug content (Schmitt et al., 2019) for a larger set of compounds (n=41) showing a very good predictivity. Using the lysosomal marker lipid bis(monoacylglycero)-phosphate (BMP), we estimated the lysosomal volume fraction for all major tissues in the rat ranging from 0.03% for adipose up to 5.3% for spleen. The pH-driven lysosomal trapping was then estimated and fully integrated into the mechanistic distribution model published by Rodgers et al. (2005). Predictions of Kpu improved for all lysosome rich tissues. For instance Kpu increased for nicotine 4-fold (spleen) and 2-fold (lung and kidney) and for quinidine 1.8-fold (brain). Although for most other drugs the effects were much less (≤ 7%).

Overall, the effect was strongest for basic compounds with a lower lipophilicity such as nicotine where the Vuss prediction changed from 1.34 to 1.58 L/kg. For more lipophilic (basic) compounds or those which already show strong interactions with acidic phospholipids the additional contribution of lysosomal trapping was less pronounced. Nevertheless, lysosomal trapping will affect intracellular distribution also of such compounds.

DMD Fast Forward. Published on November 4, 2020 as DOI: 10.1124/dmd.120.000161
This article has not been copyedited and formatted. The final version may differ from this version.

4. Significance Statement

The estimation of the lysosomal content in all body tissues facilitated the incorporation of lysosomal sequestration into a general PBPK model leading to improved predictions as well as elucidating its influence on tissue- and subcellular distribution in the rat.

DMD Fast Forward. Published on November 4, 2020 as DOI: 10.1124/dmd.120.000161
This article has not been copyedited and formatted. The final version may differ from this version.

5. Introduction

Many basic lipophilic drugs exhibit a deep distribution reflected in high volumes of distribution (Vss). The partitioning into individual tissues can however differ considerably and it is not possible to deduce this from the volume of distribution. Furthermore, experimental determination of tissue partition coefficients (Kp) is not a standard in drug discovery as it is very resource intensive. Therefore, the development of mechanistic models that are based on the tissue composition of the body and the physicochemical properties of the drug was instrumental to enable early estimation of drug distribution in drug discovery and development.

Poulin and Theil (2000) pioneered the mathematical description of partition processes into tissue water, proteins and neutral lipids focusing on the neutral drug molecules. Later, Rodgers and Rowland expanded the tissue composition based distribution equations by inclusion of drug ionisation and the resulting interaction of the charged drug species with proteins and membrane constituents (Rodgers et al., 2005; Rodgers and Rowland, 2006). In these models, the dominant affinity of the charged species of basic drugs ($pk_a > 7$) is considered to be acidic phospholipids in the tissue (Yata et al., 1990). Predictions for neutral and acidic drugs are far more accurate than for basic drugs (Chan et al., 2018), suggesting further processes being involved in the distribution of bases which are so far not accounted for. A potential additional mechanism is extensive pH-driven sequestration into lysosomes which can lead to enormous concentrations within the lysosome (up to 160,000-fold compared to the cytosol (MacIntyre and Cutler, 1988a; MacIntyre and Cutler, 1988b)). In our previous work we have shown the huge impact this has on the intracellular distribution in rat hepatocytes with lysosomes holding > 50% of the intracellular drug (Schmitt et al., 2019): Lysosomal trapping may therefore also have the potential to influence overall tissue distribution and may further improve predictions of tissue distribution for basic drugs.

While lysosomal abundance is qualitatively known in some tissues (de Duve et al., 1974; Blouin et al., 1977) for quite some time, the parameterisation needed for a PBPK model is

still challenging as their size is highly variable in different cell types (Bandyopadhyay et al., 2014). There has been a first approach to incorporate lysosomal sequestration in lung, kidney and liver using published data on lysosomal volume fractions and pH of their main cell types (Assmus et al. (2017). This model can only be applied to well-studied tissues and does not cover other lysosome rich tissues such as spleen, brain and gut. In order to be able to include lysosomal trapping in all body tissues a surrogate for the lysosomal size is required, e.g. by a marker that is unique for lysosomes. BMP, a lipid exclusively found in the luminal side of the endo-/lysosomal membrane, is responsible for endo-/lysosomal stabilization and fusion, it promotes hydrolysis by enhancing adhesion of enzymes and activator proteins to the inner lysosomal membrane and cholesterol transport (Schulze et al., 2009; Gallala and Sandhoff, 2011; Hullin-Matsuda et al., 2014). The involvement in many essential lysosomal processes makes its abundance a good surrogate for the size of the endo-/lysosomal system. We have recently published BMP concentrations in all major rat tissues (Wang & Schmitt et al., 2019), thereby providing reliable estimates of the size of the lysosomal system in these tissues. This knowledge allows for a new possibility to include lysosomal trapping into overall tissue distribution predictions.

The aim of this study was to further expand the mechanistic equations of Rodgers et al. (2005) by inclusion of lysosomal sequestration as an additional distribution process for basic drugs ($pk_a > 7$). We have validated our previously published approach to predict the intracellular drug distribution to lysosomes in rat hepatocytes (Schmitt et al., 2019) for a broad set of compounds, estimated the size of the lysosomal compartment in various rat tissues and integrated both into the mechanistic equations to predict tissue partitioning. Impact on Kpu was evaluated comparing prediction results to the original model and experimental data of the original dataset of 28 basic compounds (Rodgers et al., 2005). The *in vivo* distribution of 13 protein kinase inhibitors (PKI) extending the physicochemical property space of the original dataset was used to further investigate the performance of both models and to evaluate the influence of lysosomal trapping on Kpu and Vuss.

DMD Fast Forward. Published on November 4, 2020 as DOI: 10.1124/dmd.120.000161
This article has not been copyedited and formatted. The final version may differ from this version.

6. Materials & Methods

Chemicals and Reagents

Afatinib, axitinib, bosutinib, cediranib, crizotinib, dasatinib, erlotinib, gefitinib, ibrutinib, lapatinib, linsitinib, masitinib, motesanib, nilotinib, nintedanib, olaparib, pazopanib, quizartinib, saracatinib, selumetinib, sunitinib, tandutinib, vandetanib were purchased from Selleck Chemicals LLC (Houston, TX, USA). Imatinib was purchased from Enzo Life Sciences (ELS) AG (Lausen, GER) and regorafenib was obtained from Bayer AG (Berlin, GER). Monensin sodium was bought from Sigma Aldrich (St. Louis, MO). Acetonitrile and methanol were purchased from Honeywell Specialty Chemicals Seelze GmbH (Seelze, Germany).

Animals and treatment

Male Han:Wistar rats (Envigo, Netherlands / Janvier Laboratories, France) of 300 ± 30 g body weight were used. Animals were housed in groups of up to three in transparent standard cages at 22° C with a 12 h light/dark cycle. Standard rat diet and water were provided *ad libitum*.

Direct quantification of lysosomal drug content

The lysosomal drug content was measured in rat hepatocytes as described in Schmitt et al. (2019). In short, rat hepatocytes were isolated, purified, seeded on 24-well collagen coated plates and subsequently incubated for 24 h resulting in greatly reduced transporter expression as well as metabolic enzyme activity. Drug accumulation of compounds was measured (i) in cultured control hepatocytes and (ii) in hepatocytes with inactivated lysosomes (+ 25 µM monensin). Samples were analysed via LC/MS-MS and the lysosomal drug content was calculated by the difference of accumulation in the cells. The lysosomal drug content was measured for a set of 26 test compounds at a low concentration of 5 µM to avoid lysosomal saturation during the experiments (Schmitt et al., 2019). Experimental determination of the lysosomal drug content was done extensively (n=9) for nine compounds

DMD Fast Forward. Published on November 4, 2020 as DOI: 10.1124/dmd.120.000161
This article has not been copyedited and formatted. The final version may differ from this version.

with expected low, medium and high potential for lysosomal trapping; other compounds were each measured twice.

Prediction of lysosomal drug sequestration

The extent of lysosomal sequestration L for drugs was calculated as previously described in Schmitt et al. (2019) using the following equation:

$$L = \int_{pH_{min}}^{pH_{cyto}} \frac{V(pH) \cdot K_L\left(pH, pK_{a,1}, pK_{a,2}\right)}{V_B}\, dpH \qquad (1)$$

with $V(pH)$ as the volume of the lysosomal compartment at a given pH, $K_L$as the concentration ratio of compound between the cytosol and the lysosome in dependency on the lysosomal pH from pH_{min} = 4 up to pH_{cyto}= 7.2, as well as the most and second most basic drug moiety as described by MacIntyre and Cutler (1988a). V_B represents the volume of the non-acidic compartment in a hepatocyte. The extent of lysosomal sequestration L was expressed as the percentage in lysosomes of the total drug in the cells. Correlation of predictions and experimental results were carried out in OriginPro 2018.

Size of the endo-/lysosomal system in rat tissues

The fractional volume of lysosomes in the liver was estimated from the extensively characterised rat hepatocytes (Schmitt et al., 2019) under the simplification of hepatocytes being the only cell type in this tissue as they make up about 93 % of the cellular tissue in the liver (Blouin et al., 1977). Considering the cellular space makes up 84.1 % of the liver (Blouin et al., 1977) a fractional tissue volume of 1.3 % could be calculated for lysosomes. Lysosomal abundance for other tissues was calculated relatively to the liver based on the concentration of the lysosomal specific marker lipid BMP (Schulze et al., 2009; Gallala and Sandhoff, 2011; Hullin-Matsuda et al., 2014), which were recently determined by Wang & Schmitt et al. (2019) (Table 2). As BMP levels of bone, pancreas and thymus were not measured, no lysosomal compartment could be calculated for these tissues.

DMD Fast Forward. Published on November 4, 2020 as DOI: 10.1124/dmd.120.000161
This article has not been copyedited and formatted. The final version may differ from this version.

Lysosomal sequestration in the prediction of drug tissue distribution

The proposed equation to predict tissue distribution of basic-lipophilic drugs of Rodgers et al. (2005) considers the pH-driven accumulation in the intracellular water (IW), distribution to the extracellular water (EW) and the association to neutral (phospho-)lipids (NPL / NL) as well as acidic phospholipids (AP^-):

$$Kpu_{R\&R} = \left(\frac{1 + 10^{pK_a - pH_{IW}}}{1 + 10^{pK_a - pH_p}} \cdot f_{IW}\right) + f_{EW} + \left(\frac{K_a \cdot [AP^-]_T \cdot 10^{pK_a - pH_{IW}}}{1 + 10^{pK_a - pH_p}}\right) + \left(\frac{P \cdot f_{NL} + (0.3P + 0.7) \cdot f_{NP}}{1 + 10^{pK_a - pH_p}}\right) \quad (2)$$

with $f_{IW}, f_{EW}, f_{NL}, f_{NP}$ as fractional volumes of the tissue, $pH_{IW} = 7.0$ and $pH_p = 7.4$ as the pH of the intracellular water and the plasma, pK_a as the compounds acid dissociation constant, K_a as the association constant of the compound to acidic phospholipids with the tissue concentration $[AP^-]_T$. K_a is estimated from the compounds blood:plasma ratio as described by Rodgers et al. (2005).

With the absence of active transport processes and the steady-state condition in the model, the concentration of the unprotonated base is equal in each compartment, thus allowing the lysosomes to be put into a direct relation to the plasma for estimating the pH-driven sequestration as followed:

$$\mathrm{Kpu} = \left(\frac{1 + 10^{pK_a - pH_{IW}}}{1 + 10^{pK_a - pH_p}} \cdot f_{IW}\right) + f_{EW} + \left(\frac{K_a \cdot [AP^-]_T \cdot 10^{pK_a - pH_{IW}}}{1 + 10^{pK_a - pH_p}}\right) + \left(\frac{P \cdot f_{NL} + (0.3P + 0.7) \cdot f_{NP}}{1 + 10^{pK_a - pH_p}}\right) + \left(\frac{1 + 10^{pK_a - pH_L}}{1 + 10^{pK_a - pH_p}} \cdot f_{Lyso}\right) \quad (3)$$

with f_{Lysp} as the fractional volume of lysosomes in the respective tissues and $pH_L = 5.3$ as an effective pH across all lysosomes, derived from eq. (1) for monobasic drugs under consideration of the complete pH-profile in rat hepatocytes. All processes accommodated in the mechanistic equation are depicted in Figure 1.

DMD Fast Forward. Published on November 4, 2020 as DOI: 10.1124/dmd.120.000161
This article has not been copyedited and formatted. The final version may differ from this version.

The unbound volume of distribution was calculated according to Rodgers and Rowland (2007) by:

$$Vu_{ss} = \frac{V_P}{fu} + \sum V_{T,i} \cdot Kpu_i \quad (4)$$

with *Vp as the plasma volume,* Vu_{ss} as the unbound volume of distribution at steady state, fu as the unbound fraction of drug in plasma, $V_{T,i}$ as the volume of individual tissues and Kpu_i as the partitioning in tissues, defined as the ratio of the total concentration in the tissue to the unbound plasma concentration, calculated by equation (3).

Tissue specific input parameters

Parameters to predict the unbound tissue partitioning and the unbound volume of distribution in rats were adopted from Rodgers et al. (2005) and Rodgers and Rowland (2007) with the exception of the intracellular water, which was reduced by the newly defined lysosomal compartment (Table 1).

Compound specific parameters

Parameters for the original set of compounds by Rodgers & Rowland were taken from literature (Rodgers and Rowland, 2007). Timolol was excluded from the comparison as our model is only valid for mono-basic compounds, while R&R treated it as a di-basic compound, i.e. with two highly basic pKa values.

The acid dissociation constants of basic drug moieties and the drug lipophilicity of protein kinase inhibitors were predicted *in silico* using ADMET Predictor™ (Simulations Plus Inc.). Blood to plasma ratio (B:P), unbound fraction in plasma (fu) and *in vivo* volume of distribution at steady state (Vss) were determined experimentally unless published elsewhere.

B:P-Ratio

Blood of Han:Wistar Rats was drawn with K-EDTA as an anticoagulant prior to the experiment. The fresh blood of three individual rats was pooled and kept at 37 °C. Blood working solutions were prepared from DMSO stock solutions with final concentrations of 0.3 µM and 3 µM which were subsequently incubated for 15 min at 37 °C. Samples of blood

DMD Fast Forward. Published on November 4, 2020 as DOI: 10.1124/dmd.120.000161
This article has not been copyedited and formatted. The final version may differ from this version.

(n=3) were drawn for LC-MS/MS analysis. Plasma was obtained by centrifuging the blood at 3700 rpm for 15 min and samples (n=3) were drawn for LC-MS/MS analysis. Four times the volume of MeOH/IS was added to each sample for protein precipitation prior to analysis. The mean B:P-ratio was calculated from plasma and blood samples from both working concentrations.

Plasma protein binding

Plasma protein binding was measured by equilibrium dialysis according to Banker et al. (2003) with slight changes. In short, drugs were diluted into pooled rat plasma (n=4) and dialysis buffer (n=3) to final concentrations of 3 µM for the equilibrium dialysis and into plasma vials (n=3) to investigate compound stability. Samples were drawn after 7 h incubation at 37 °C. Four times the volume of MeOH was added for protein precipitation. Samples were centrifuged at 3700 rpm for 15 min and subsequently analysed via LC-MS/MS. Volume shift was corrected for by a factor of 1.09 for all compounds.

In vivo pharmacokinetic studies

To reduce animal experiments to a minimum, rat volume of distribution was gathered primarily from assessment reports of the FDA, EMA and TGA as well as from scientific articles.

The *in vivo* PK studies of cediranib, imatinib, masitinib and tandutinib were carried out in catheterised Han:Wistar rats (n=3). Application solutions were prepared in either plasma or diluted PEG400 based formulations. The doses of 0.3 – 0.5 mg/kg were administered intravenously into the tail vein. Heparinized blood samples were drawn after 2 min, 8 min, 15 min, 30 min, 45 min, 1 h, 2 h, 4 h, 7 h and 24 h and plasma was generated by centrifugation at 3700 rpm for 5 min. Samples ≤ 60 min and the application solution were additionally diluted 1:10 in rat plasma. A calibration curve was prepared in the range of 0.25 nM to 5 µM. To each sample five times the volume of acetonitrile containing internal standard was added and subsequently centrifuged at 3700 rpm for 15 min prior to LC-MS/MS analysis. Pharmacokinetic calculations were done with WinNonlin (Phoenix™, version 6.1).

DMD Fast Forward. Published on November 4, 2020 as DOI: 10.1124/dmd.120.000161
This article has not been copyedited and formatted. The final version may differ from this version.

Analytical method

Samples were analysed with liquid chromatography-tandem mass spectrometry using an Agilent 1290 Infinity System comprising a G4220A binary pump, a G1316C column compartment and G7167B multisampler linked to an AB Sciex API4000 / API5500 mass spectrometer with electrospray ionization. All compounds were detected in positive or negative MRM mode against internal standard. MRM transitions are listed in Table S1. An Ascentis® Express C18 column (30 x 2.1 mm, 2.7 µm particle size) was used with mobile phases (A) water and (B) acetonitrile with either 0.1 % acetic acid or 0.1 % ammonia. Gradients for high performance liquid chromatography are listed in Table S2.

DMD Fast Forward. Published on November 4, 2020 as DOI: 10.1124/dmd.120.000161
This article has not been copyedited and formatted. The final version may differ from this version.

7. Results

Prediction of lysosomal drug sequestration in rat hepatocytes

Our previous studies showed good predictability of lysosomal sequestration in rat hepatocytes for propranolol and imipramine (Schmitt et al., 2019). To further confirm the reliability of these predictions, the distribution into lysosomes of rat hepatocytes was measured experimentally as well as predicted *in silico* for a broad set of compounds. These PKIs comprised a broad range of physicochemical properties. With a logP of 1.6 to 6.6, all compounds possessed enough lipophilicity to cross the lipid bilayer by passive diffusion, thus being able to reach the inner acidic compartment of lysosomes - a prerequisite to undergo lysosomal trapping. The basicity of compounds ranged from a pK_a of 0.2 up to 9.7 with some of the compounds possessing a second weakly basic moiety. All physicochemical properties used to predict the lysosomal sequestration of the compounds are summarized in Table S3.

The predictions for compounds not showing any tendency for lysosomal trapping were correctly confirmed by the experimental results (Figure 2). Strong lysosomal accumulation (≥ 50 %) was well predicted with only slight deviations from the experimental results. Only Saracatinib, with 50 % of the drug trapped in lysosomes was markedly below the predicted 69 %. As lysosomal trapping increases exponentially in the range of pKa ≈ 6.5 – 7.5 predictions of moderately lysosomotropic compounds (≈ 20 – 40 % in lysosomes) showed higher deviations from experimental results with increasing basicity. Besides good predictions for gefitinib and dasatinib, crizotinib and tandutinib were both overpredicted by about 25 % and lapatinib was underpredicted by 24 % (Figure 2 A). Statistical analysis showed a linear relationship between predicted and experimentally determined lysosomal sequestration for this diverse set of compounds with a correlation coefficient of $r^2 = 0.8$ and no systematic over- or underprediction (Figure 2 B). 68 % of the compounds had a total deviation of < 10 % and 86 % of < 15 %. With lysosomes having a significant influence on intracellular distribution of basic lipophilic drugs, the incorporation of pH-driven sequestration

DMD Fast Forward. Published on November 4, 2020 as DOI: 10.1124/dmd.120.000161
This article has not been copyedited and formatted. The final version may differ from this version.

into the mechanistic distribution equation of Rodgers et al. (2005) should further improve prediction results.

Estimation of the size of the endo-/lysosomal system in rat tissues via BMP content

Lysosomal content was calculated based on the lysosome specific marker lipid BMP (see materials & method section). The lysosomal content varies greatly between the different tissues. Adipose, muscle and skin tissue have only little BMP content which calculates to few lysosomes with fractional tissue volumes between 0.03 – 0.16 %, followed by the heart with 0.32 %. Most tissues have a similar modest calculated fractional volume of lysosomes as the liver of about 1 – 1.7 %. The spleen however has by far the most lysosomes based on the relative BMP content with a fractional volume of 5.3 % (Table 2). For the first time, we have estimated the size of the lysosomal system across many body tissues. This fulfils the main prerequisite to be able to incorporate pH-driven lysosomal sequestration in the mechanistic approach to predict drug tissue distribution.

Prediction of drug tissue distribution including lysosomal sequestration in all rat tissues

We have extended the mechanistic model by Rodgers and Rowland (2007) to predict drug tissue distribution by inclusion of tissue specific lysosomal compartments. As the model assumes an equal distribution of the unprotonated free base across all compartments, the pH-driven lysosomal partitioning can be calculated from plasma concentrations. For simplification, an effective lysosomal pH was derived from equation (1), which could reliably predict the lysosomal distribution of a large set of compounds in rat hepatocytes. The effective pH comprises the information gained from the full pH-profile and should not be mistaken for the widely used average lysosomal pH.

To examine the influence of this addition, the original dataset of basic lipophilic drugs was predicted with the equation according to Rodgers et al. (2005) and the newly developed lysosomal extended equation (3).

DMD Fast Forward. Published on November 4, 2020 as DOI: 10.1124/dmd.120.000161
This article has not been copyedited and formatted. The final version may differ from this version.

In all tissues the Kpu increased by considering lysosomal trapping in the predictions. However, in tissues with few lysosomes like fat, heart, muscle and skin only by 1 - 3 % on average. Due to the considerably greater size of the endo-/lysosomal system in intestine, kidney, liver and lung predictions of Kpu increased by about 10 % on average. With 29 % and 43 % for brain and spleen respectively, lysosomal sequestration showed the biggest impact on those tissues (Table 3), showing a large spread depending on compound specific properties. Nicotine, for instance, was predicted about 300 % higher in spleen and 100 % higher in lung and kidney, whereas Verapamil was not affected in any of these tissues. Although nicotine showed the greatest change in most of the tissues, procainamide and quinidine showed the strongest increase of 80 % in brain (Figure 3). Interestingly, stronger differences in Kpu changes between compounds were seen in brain and spleen, than in other lysosomal rich tissues like kidney, liver or lung. In tissues with few lysosomes, the Kpu prediction did not change notably for any compound. Deviations to experimental Kpu values did not significantly change for tissues with few lysosomes but improved for all lysosome rich tissues compared to Rodgers et al. (2005). Detailed prediction results including Kpu values for all compounds across tissues are summarised in Table S4. Incorporating lysosomal trapping into the mechanistic equation led to an overall improvement of the predictions for drug tissue partition.

Tissue distribution of protein kinase inhibitors

The effect of lysosomal trapping on tissue distribution was further examined with 13 PKIs which showed moderate to strong lysosomal sequestration in rat hepatocytes and could successfully be predicted by equation (1). Those compounds were predicted using the original equation by Rodgers et al. (2005) as well as the lysosomal extended equation (3). Due to the lack of experimental tissue Kpu values for those compounds, the unbound volume of distribution (Vuss) was used as distribution parameter to assess the quality of predictions. The data were primarily collected from literature and complemented by in vivo PK studies (Table 4). The lipophilicity of the tested compounds ranged from logP 3 to 5, all exceeding the recommended lipophilicity of Rodgers and Rowland (2007) of logP < 3. Additionally, the

DMD Fast Forward. Published on November 4, 2020 as DOI: 10.1124/dmd.120.000161
This article has not been copyedited and formatted. The final version may differ from this version.

compounds showed a larger spread in their B:P-ratios compared to the original dataset. With a B:P-ratio of 0.48, lapatinib does hardly partition into blood cells, whereas tandutinib with a B:P ratio of 2.8 has a preference to distribute into blood cells.

The predictions for Vuss covered a wide range from 76 L/kg up to 1085 L/kg. Tandutinib, cediranib and bosutinib showed the lowest Vuss with 76 L/kg, 90 L/kg and 93 L/kg, respectively. Most of the compounds were predicted to have Vuss between 100 L/kg and 300 L/kg. However, sunitinib, masitinib and lapatinib exceeded this range with 375 L/kg, 411 L/kg and 1085 L/kg, respectively (Table 4). The prediction of Vuss did not change notably by including lysosomal trapping into the predictions. Results predicted according to the lysosomal extended equation (3) only differed by up to 1 L/kg compared to the model by Rodgers et al. (2005) (Table S5). On average, predictions of Vuss deviated from experimental results only by 1.7-fold, with cediranib and sunitinib showing the highest deviation of 2.2-fold (Figure 6).

DMD Fast Forward. Published on November 4, 2020 as DOI: 10.1124/dmd.120.000161
This article has not been copyedited and formatted. The final version may differ from this version.

8. Discussion

Current distribution models do not, or only partially consider lysosomal sequestration which is particularly important for basic lipophilic drugs (Poulin and Theil, 2002; Rodgers et al., 2005, Assmus et al., 2017). To close this gap, we have validated our previously published *in silico* prediction of lysosomal trapping in rat hepatocytes (Schmitt et al., 2019) and used this approach, in combination with published BMP tissue levels as maker lipid for the endo/lysosomal system in the body tissues of the rat (Wang & Schmitt et al., 2019), to predict Kpu and Vuss for the original dataset from Rodgers et al. (2005). Comparison of the results allowed to evaluate the overall impact of lysosomal sequestration on these PK parameters. The predictivity of the approach was further examined using a set of more lipophilic PKIs whose physicochemical properties are beyond the previous range reflecting a more recent druglike space.

Prediction of lysosomal trapping

The more diverse dataset in the present study (Figure 2) confirms the high predictivity of our previously published approach to predict lysosomal trapping (Schmitt et al., 2019). As reported for propranolol and imipramine (Schmitt et al., 2019), the superiority of using the full pH profile of the endo-lysosomal system instead of simply using an average lysosomal pH value was also found for PKIs. The absolute deviation of predictions from experimental results was reduced from 12% to 6 % (data not shown), and the number of underpredicted compounds went down by one third from 18 to 12. The underestimation for Lapatinib (20 % instead of 44 %) may be explained by the predicted pK_a = 6.5 that was used for Lapatinib. An alternative software (Chemaxxon, Chemaxxon Ltd.) which estimates a pK_a of 7.2 would predict a lysosomal sequestration of 40 % which is fully in line with the experimental observation and highlights the impact of the pK_a estimates.

DMD Fast Forward. Published on November 4, 2020 as DOI: 10.1124/dmd.120.000161
This article has not been copyedited and formatted. The final version may differ from this version.

Lysosomal sequestration in the prediction of drug tissue partition

With no quantified BMP in red blood cells, lysosomes are not expected in this cell type which is in line with the absence of any information on lysosomes in an extensive review on red blood cells given by (Hinderling, 1997). Accordingly, the estimation of Ka, the association constant of the compound for acidic phospholipid from the blood-to-plasma ratio, as recommended by Rodgers et al. (2005) still holds. The incorporation of the lysosomal sequestration into the mechanistic equation revealed tissue dependent effects on Kpu. Adipose tissue, muscle and heart were minimally affected due to the low abundance of lysosomes. However, for lysosome rich tissues such as kidney, spleen and liver which are generally underpredicted by Rodgers et al. (2005) up to 4-fold higher Kpu values (e.g. nicotine/spleen) were observed leading to improved predictions. In total about 27 % (vs. 23 %) of the 245 predicted Kpu values were within 1.25-fold of the experimental results. Predictions within 2-fold were achieved for 63 % (vs. 60 %) of the Kpu values, while false predictions with deviations of greater 4-fold were reduced to 9 % (vs. 11 %).

For compounds like nicotine, Kpu was strongly affected by lysosomal trapping with a contribution of up to 50% of the liver Kpu (Table 5) suggesting significant partitioning into lysosomes and intracellular water but low tissue binding. These compounds share a high basicity, relatively low lipophilicity and a low B:P-ratio (Figure 4). In contrast tissue distribution of compounds with similar pK_a but higher lipophilicity and B:P ratio is clearly dominated by lipid partitioning, in particular phospholipid binding with little overall contribution by lysosomal trapping. For example, despite showing strong lysosomal trapping, the Kpu of propranolol in the liver is almost entirely governed by its affinity for acidic phospholipids (>99%, Table 5).

Despite the strong effect of lysosomal trapping on Kpu predictions for some compounds in some tissues, there was only a marginal impact on Vuss. On average Vuss predictions increased by 3 %, thus not significantly changing compared to Rodgers et al. (2005) (Figure 5). Lysosome rich tissues in which Kpu changes were observed tend to have rather small

tissue volumes (Table 1). Spleen, with only 0.83 ml in rat, the lysosome richest tissue, does not contribute much to Vuss as it represents only ~0.3 % of the body volume. Furthermore, tissue distribution not only depends on lysosomal trapping but also on tissue binding.

Our liver model does not take into account sequestration by Kupffer cells that may contain even more lysosomes than hepatocytes (Blouin et al., 1977). Despite their low abundance (~2 % of liver) they may also contribute to lysosomal sequestration by this organ. However, because data on their overall lysosomal content are not available, we could not include this cell types into our model. Furthermore, our model focuses on lysosomal trapping by pH-partitioning and does not cover interactions of drugs with the lysosomal membrane which may also be relevant (Colombo and Bertini, 1988; Hallifax and Houston, 2007). There are two key differences between the approach taken here and that taken by Assmus et al. (2017). First, while they cover lysosomal sequestration in lung, liver and kidney, our method incorporates the lysosomal content of all tissues in the body, in particular spleen, brain and gut which are also rich in lysosomes. Second, the lysosomal sequestration as estimated by Assmus et al. is effectively driven by interactions with lysosomal membranes, thus emphasizing lysosomal binding, that is calculated in analogy to the plasma membrane binding and hence tends to result in overpredictions as already reported by (Nigade et al., 2019). From our perspective, using the plasma membrane as a surrogate as applied by Assmus et al. is arguable as the lysosomal membrane differs greatly in its composition (Amanuma-Muto et al., 1983; Kobayashi et al., 2002; Schulze et al., 2009). Furthermore, the acidic phospholipid phosphatidylserine, which is an important binding site for basic drugs, is located on the cytosolic side of the lysosomal membrane (Hullin-Matsuda et al., 2014) and is thus not able to interact with compounds inside of the lysosome. As no data on lysosomal membrane composition are available, our approach applies pH driven lysosomal trapping only. Lysosomal membrane binding can only be included once quantitative data of lysosomal membrane composition become available.

DMD Fast Forward. Published on November 4, 2020 as DOI: 10.1124/dmd.120.000161
This article has not been copyedited and formatted. The final version may differ from this version.

Tissue distribution of protein kinase inhibitors

We have selected this class of drugs to evaluate the performance of our model as their physico-chemical properties, especially the lipophilicity (logP = 3 - 5), are beyond the range of the original dataset tested by Rodgers et al. (2005). Reliable predictions for such compound classes will help to guide lead optimization and facilitate PK projections to human (Reichel and Lienau, 2016; Petersson et al., 2019). The extended model was applied to predict the tissue Kpu's and Vuss of these mainly basic PKIs (Table 4). With intracellular distribution to lysosomes of up to 66 % in hepatocytes, this mechanism is expected to have an influence on the intracellular drug distribution. At the level of the predicted Kpu values, however, there was no significant change across tissues compared to the model of Rodgers et al. (2005) (Table S5). This highlights once more that although strong lysosomal trapping may occur, tissue partitioning of basic lipophilic compounds seems to be mainly driven by membrane binding, in particular to acidic phospholipids.

Although lysosomal trapping may not be significantly contributing to Kpu of all basic lipophilic drugs, it cannot be neglected as mechanism of intracellular drug distribution ultimately affecting drug safety and efficacy (Smith et al., 2010, Guo et al., 2018). Indeed, the unbound intracellular concentrations which drive engagement of intracellular drug targets (Trünkle et al., 2020) can be influenced by lysosomal trapping as recently demonstrated by Llanos et al. (2019) causing the prolonged activity of Palbociclib.

Conclusion

We have extended the mechanistic, tissue composition-based equations to predict tissue distribution by inclusion of lysosomal compartments for all body tissues of the rat, thereby further improving the predictivity of Kpu for basic drugs undergoing lysosomal trapping. We see our model as another step in the continuing evolution of tissue distribution models, starting with the seminal work by Poulin and Theil (2002) focusing on mechanisms related to the passive drug distribution of neutral molecules between aqueous/lipids/proteins in plasma and tissues, that was subsequently advanced by Rodgers et al. (2005) to also include ionic

DMD Fast Forward. Published on November 4, 2020 as DOI: 10.1124/dmd.120.000161
This article has not been copyedited and formatted. The final version may differ from this version.

interactions of charged molecules with acidic phospholipids, and more recently by Assmus et al. (2017) to model lysosomal trapping in three organs. Our model extension now covers pH related lysosomal trapping in all major tissues of the rat and is likely extendable to other animal species, as well as to human. Direct comparison with the dataset by Rodgers et al. (2007) showed an improvement of Kpu predictions which however was smaller than expected for basic lipophilic drugs. This finding was confirmed for a set of PKIs showing that Kpu and Vuss were not significantly changed for of these lipophilic basic compounds, mainly due to the very small lysosomal volume even in lysosome rich tissues and the much stronger impact of lipid- and acidic phospholipid binding to overall tissue distribution.

DMD Fast Forward. Published on November 4, 2020 as DOI: 10.1124/dmd.120.000161
This article has not been copyedited and formatted. The final version may differ from this version.

9. Acknowledgments

We would like to thank Stephan Menz for his assistance in mathematical questions and Daniel Trost and Martin Klein for their support in hepatocyte isolation and LC-MS/MS quantification. We are grateful to Prof. Malcolm Rowland for fruitful thoughts and discussions.

DMD Fast Forward. Published on November 4, 2020 as DOI: 10.1124/dmd.120.000161
This article has not been copyedited and formatted. The final version may differ from this version.

10. Authorship Contributions

Participated in research design: MVS, AR, GF, PL, XL

Conducted experiments: MVS

Performed data analysis: MVS, AR, PL, XL

Discussed results: MVS, AR, GF, PL, XL

Drafted manuscript: MVS, AR, PL

Wrote or contributed to the writing of the manuscript: MVS, AR, GF, PL

DMD Fast Forward. Published on November 4, 2020 as DOI: 10.1124/dmd.120.000161
This article has not been copyedited and formatted. The final version may differ from this version.

11. References

Amanuma-Muto K, Kanaseki T, Imanaka T, Ohkuma S, and Takano T (1983) Lipid composition of low-density lysosomal membrane fraction prepared from atheromatous aorta of cholesterol-fed rabbits. *Biochemistry international* **7:**107-114.

Assmus F, Houston JB, and Galetin A (2017) Incorporation of lysosomal sequestration in the mechanistic model for prediction of tissue distribution of basic drugs. *Eur J Pharm Sci* **109:**419-430.

Bandyopadhyay D, Cyphersmith A, Zapata JA, Kim YJ, and Payne CK (2014) Lysosome transport as a function of lysosome diameter. *PloS one* **9:**e86847.

Banker MJ, Clark TH, and Williams JA (2003) Development and validation of a 96-well equilibrium dialysis apparatus for measuring plasma protein binding. *Journal of pharmaceutical sciences* **92:**967-974.

Blouin A, Bolender RP, and Weibel ER (1977) Distribution of organelles and membranes between hepatocytes and nonhepatocytes in the rat liver parenchyma. A stereological study. *The Journal of Cell Biology* **72:**441-455.

Chan R, De Bruyn T, Wright M, and Broccatelli F (2018) Comparing Mechanistic and Preclinical Predictions of Volume of Distribution on a Large Set of Drugs. *Pharmaceutical research* **35:**87.

Colombo MI and Bertini F (1988) Properties of binding sites for chloroquine in liver lysosomal membranes. *Journal of cellular physiology* **137:**598-602.

de Duve C, de Barsy T, Poole B, Trouet A, Tulkens P, and Van Hoof F (1974) Commentary. Lysosomotropic agents. *Biochemical pharmacology* **23:**2495-2531.

EMA (2006) Scientific discussion Sutent in: *Sunitinib*, European Medicines Agency, Europa.

EMA (2008a) Assessment Report for Iressa, EMEA/CHMP/563746/2008, EMEA/H/C/001016, in: *Gefitinib*, European Medicines Agency, Europa.

EMA (2008b) Assessment Report for Tyverb, EMEA/302222/2008, EMEA/H/C/795, in: *Lapatinib*, European Medicines Agency, Europa.

EMA (2013) CHMP assessment report Giotrif, EMA/491185/2013, EMEA/H/C/002280, in: *Afatinib*, European Medicines Agency, Europa.

FDA (2012) Pharmacology review(s) Bosulif, 203341Orig1s000, in: *Bosutinib*, Food and Drug Administration, USA.

Gallala HD and Sandhoff K (2011) Biological function of the cellular lipid BMP-BMP as a key activator for cholesterol sorting and membrane digestion. *Neurochemical research* **36:**1594-1600.

Guo Y, Chu X, Parrott NJ, Brouwer KLR, Hsu V, Nagar S, Matsson P, Sharma P, Snoeys J, Sugiyama Y, Tatosian D, Unadkat JD, Huang SM, Galetin A, and International Transporter C (2018) Advancing Predictions of Tissue and Intracellular Drug Concentrations Using In Vitro, Imaging and Physiologically Based Pharmacokinetic Modeling Approaches. *Clinical pharmacology and therapeutics* **104:**865-889.

Hallifax D and Houston JB (2007) Saturable uptake of lipophilic amine drugs into isolated hepatocytes: mechanisms and consequences for quantitative clearance prediction. *Drug metabolism and disposition: the biological fate of chemicals* **35:**1325-1332.

Hennequin LF, Allen J, Breed J, Curwen J, Fennell M, Green TP, Lambert-van der Brempt C, Morgentin R, Norman RA, Olivier A, Otterbein L, Ple PA, Warin N, and Costello G (2006) N-(5-chloro-1,3-benzodioxol-4-yl)-7-[2-(4-methylpiperazin-1-yl)ethoxy]-5- (tetrahydro-2H-pyran-4-yloxy)quinazolin-4-amine, a novel, highly selective, orally available, dual-specific c-Src/Abl kinase inhibitor. *Journal of medicinal chemistry* **49:**6465-6488.

Hinderling PH (1997) Red blood cells: a neglected compartment in pharmacokinetics and pharmacodynamics. *Pharmacological reviews* **49:**279-295.

Hullin-Matsuda F, Taguchi T, Greimel P, and Kobayashi T (2014) Lipid compartmentalization in the endosome system. *Seminars in cell & developmental biology* **31:**48-56.

Kamath AV, Wang J, Lee FY, and Marathe PH (2008) Preclinical pharmacokinetics and in vitro metabolism of dasatinib (BMS-354825): a potent oral multi-targeted kinase inhibitor against SRC and BCR-ABL. *Cancer chemotherapy and pharmacology* **61:**365-376.

Kobayashi T, Beuchat MH, Chevallier J, Makino A, Mayran N, Escola JM, Lebrand C, Cosson P, Kobayashi T, and Gruenberg J (2002) Separation and characterization of late endosomal membrane domains. *The Journal of biological chemistry* **277:**32157-32164.

Llanos S, Megias D, Blanco-Aparicio C, Hernandez-Encinas E, Rovira M, Pietrocola F, and Serrano M (2019) Lysosomal trapping of palbociclib and its functional implications. *Oncogene* **38:**3886-3902.

Lombardo LJ, Lee FY, Chen P, Norris D, Barrish JC, Behnia K, Castaneda S, Cornelius LA, Das J, Doweyko AM, Fairchild C, Hunt JT, Inigo I, Johnston K, Kamath A, Kan D, Klei H, Marathe P, Pang S, Peterson R, Pitt S, Schieven GL, Schmidt RJ, Tokarski J, Wen ML, Wityak J, and Borzilleri RM (2004) Discovery of N-(2-chloro-6-methyl- phenyl)-2-(6-(4-(2-hydroxyethyl)-piperazin-1-yl)-2-methylpyrimidin-4- ylamino)thiazole-5-carboxamide (BMS-354825), a dual Src/Abl kinase inhibitor with potent antitumor activity in preclinical assays. *Journal of medicinal chemistry* **47:**6658-6661.

MacIntyre AC and Cutler DJ (1988a) The potential role of lysosomes in tissue distribution of weak bases. *Biopharmaceutics & drug disposition* **9:**513-526.

MacIntyre AC and Cutler DJ (1988b) Role of lysosomes in hepatic accumulation of chloroquine. *Journal of pharmaceutical sciences* **77:**196-199.

McKillop D, Partridge EA, Hutchison M, Rhead SA, Parry AC, Bardsley J, Woodman HM, and Swaisland HC (2004) Pharmacokinetics of gefitinib, an epidermal growth factor receptor tyrosine kinase inhibitor, in rat and dog. *Xenobiotica; the fate of foreign compounds in biological systems* **34:**901-915.

Nigade PB, Gundu J, Pai KS, Nemmani KVS, and Talwar R (2019) Prediction of volume of distribution in preclinical species and humans: application of simplified physiologically based algorithms. *Xenobiotica; the fate of foreign compounds in biological systems* **49:**528-539.

O'Brien Z and Fallah Moghaddam M (2013) Small molecule kinase inhibitors approved by the FDA from 2000 to 2011: a systematic review of preclinical ADME data. *Expert opinion on drug metabolism & toxicology* **9:**1597-1612.

Petersson C, Papasouliotis O, Lecomte M, Badolo L, and Dolgos H (2019) Prediction of volume of distribution in humans: analysis of eight methods and their application in drug discovery. *Xenobiotica; the fate of foreign compounds in biological systems***:**1-10.

PMDA (2012) Review Report: Xalkori Capsules 200 mg and 250 mg, in: *Crizotinib*, Pharmaceuticals and Medical Devices Agency, Japan.

Poulin P and Theil FP (2000) A priori prediction of tissue:plasma partition coefficients of drugs to facilitate the use of physiologically-based pharmacokinetic models in drug discovery. *Journal of pharmaceutical sciences* **89:**16-35.

Poulin P and Theil FP (2002) Prediction of pharmacokinetics prior to in vivo studies. II. Generic physiologically based pharmacokinetic models of drug disposition. *Journal of pharmaceutical sciences* **91:**1358-1370.

Reichel A and Lienau P (2016) Pharmacokinetics in Drug Discovery: An Exposure-Centred Approach to Optimising and Predicting Drug Efficacy and Safety. *Handbook of experimental pharmacology* **232:**235-260.

Rodgers T, Leahy D, and Rowland M (2005) Physiologically based pharmacokinetic modeling 1: predicting the tissue distribution of moderate-to-strong bases. *Journal of pharmaceutical sciences* **94:**1259-1276.

Rodgers T and Rowland M (2006) Physiologically based pharmacokinetic modelling 2: predicting the tissue distribution of acids, very weak bases, neutrals and zwitterions. *Journal of pharmaceutical sciences* **95:**1238-1257.

Rodgers T and Rowland M (2007) Mechanistic approaches to volume of distribution predictions: understanding the processes. *Pharmaceutical research* **24:**918-933.

Schmitt MV, Lienau P, Fricker G, and Reichel A (2019) Quantitation of Lysosomal Trapping of Basic Lipophilic Compounds Using In Vitro Assays and In Silico Predictions Based on the Determination of the Full pH Profile of the Endo-/Lysosomal System in Rat Hepatocytes. *Drug metabolism and disposition: the biological fate of chemicals* **47:**49-57.

Schulze H, Kolter T, and Sandhoff K (2009) Principles of lysosomal membrane degradation: Cellular topology and biochemistry of lysosomal lipid degradation. *Biochimica et biophysica acta* **1793:**674-683.

Smith DA, Di L, and Kerns EH (2010) The effect of plasma protein binding on in vivo efficacy: misconceptions in drug discovery. *Nature Reviews Drug Discovery* **9:**929-939.

TGA (2013) Australian Public Assessment Report for vandetanib, PM-2011-03002-3-4, in: *Vandetanib*, Therapeutic Goods Administration, Australien.

Trünkle C, Lechner C, Korr D, Bouché L, Barak N, Fernández-Montalván A, Süssmuth RD, and Reichel A (2020) Concentration Dependence of the Unbound Partition Coefficient Kp(uu) and Its Application to Correct for Exposure-Related Discrepancies between Biochemical and Cellular Potency of KAT6A Inhibitors. Drug metabolism and disposition: the biological fate of chemicals 48:553-562.

Wang X, Schmitt MV, Xu L, Jiao Y, Guo L, Lienau P, Reichel A, and Liu X (2019) Quantitative molecular tissue atlas of Bis(monoacylglycero)phosphate and phosphatidylglycerol membrane lipids in rodent organs generated by methylation assisted high resolution mass spectrometry. *Anal Chim Acta* **1084:**60-70.

Yata N, Toyoda T, Murakami T, Nishiura A, and Higashi Y (1990) Phosphatidylserine as a determinant for the tissue distribution of weakly basic drugs in rats. *Pharmaceutical research* **7:**1019-1025.

DMD Fast Forward. Published on November 4, 2020 as DOI: 10.1124/dmd.120.000161
This article has not been copyedited and formatted. The final version may differ from this version.

12. Footnotes

This work was financed by Bayer AG, Germany.

DMD Fast Forward. Published on November 4, 2020 as DOI: 10.1124/dmd.120.000161
This article has not been copyedited and formatted. The final version may differ from this version.

13. Figure Legends

Figure 1: Schematic Illustration of processes included in the mechanistic equation 3 to predict tissue distribution of basic lipophilic drugs. The tissue distribution is estimated considering the sequestration into lysosomes which estimated based on the full pH-profile in hepatocytes, acidic phospholipid binding, neural (phospho)lipid binding and distribution into aqueous spaces. *Abbr.: B, Base; NL, neutral lipids; NP, neutral phospholipids; AP-, acidic phospholipids.*

Figure 2: A: Experimentally determined (triangles) and *in silico* predicted (filled circles) intracellular distribution to the lysosome of protein kinase inhibitors and reference compounds in rat hepatocytes. B: Correlation of experimental results and *in silico* predictions. Red line represents the line of unity, dark red represents the 95 % confidence band and light red represents the 80 % prediction band. Blue symbols represent the measurement in hepatocytes of n = 3 rats, grey symbols represent the measurement in hepatocytes of n = 2 rats. Data for propranolol and imipramine adopted from Schmitt et al. (2019).

Figure 3: Impact of the newly developed lysosomal trapping term on the prediction of tissue distribution of 27 basic lipophilic drugs. Data represents the fold increase of Kpu calculated by eq. 3 compared to predictions of Rodgers et al. (2005). Detailed results are summarised in Table S4.

Figure 4: Compound properties for which a higher influence of lysosomal trapping on tissue distribution can be expected. Note: Applies to lipophilic bases which passively diffuse across membranes in their unionized form.

Figure 5: In silico predicted versus experimentally determined Vuss of 27 basic lipophilic drugs. Predictions were made with the original model of Rodgers et al. (2005) (A) and with the incorporation of lysosomal trapping (B). Lines represent a factor of 2 (dashes) and 3 (dots) on either side of the line of unity (solid).

Figure 6: Relationship between *in silico* predicted (eq. 3) and *in vivo* unbound volume of distribution in rats of 13 basic-lipophilic protein kinase inhibitors. Lines represent a factor of 2 (dashes) and 3 (dots) on either side of the line of unity (solid).

DMD Fast Forward. Published on November 4, 2020 as DOI: 10.1124/dmd.120.000161
This article has not been copyedited and formatted. The final version may differ from this version.

14. Tables

Table 1: Tissue specific input parameters to predict the unbound tissue partitioning and unbound volume of distribution (Vuss) in rats, which comprises the fractional tissues volumes of Rodgers et al. (2005) extended by a lysosomal compartment.

	Fractional Tissue Volume[a]					Tissue Concentration of APL [mg/g]	Tissue Volume
Tissue	NL	NPL	EW	IW[b]	Lysosomes[c]		
Ref.	[d]	[d]	[d]			[d]	[e]
Blood cells	0.0017	0.0029	N.A.	0.603	n.a.	0.5	
Adipose	0.853	0.0016	0.135	0.017	0.00027	0.4	10.43
Bone	0.017	0.0017	0.1	0.346	N.D.	0.67	16.47
Brain	0.039	0.0015	0.162	0.606	0.0136	0.4	1.3
Gut	0.038	0.0125	0.282	0.463	0.0122	2.41	11.1
Heart	0.014	0.0111	0.32	0.453	0.0032	2.25	1.08
Kidney	0.012	0.0242	0.273	0.466	0.0173	5.03	2.85
Liver	0.014	0.024	0.161	0.560	0.0125	4.56	14.67
Lung	0.022	0.0128	0.336	0.431	0.0151	3.91	1.53
Muscle	0.01	0.0072	0.118	0.629	0.0011	1.53	136.24
Pancreas	0.041	0.0093	0.12	0.664	n.d.	1.67	0.94
Skin	0.06	0.0044	0.382	0.289	0.0016	1.32	43.69
Spleen	0.0077	0.0113	0.207	0.526	0.0527	3.18	0.83
Thymus	0.017	0.0092	0.15	0.626	n.d.	2.3	0.73
Plasma	-	-	-	-	n.a.	-	8.13

Abbr. NL, neutral lipids; NPL, neutral phospholipids; EW, extracellular water; IW, intracellular water; APL, acidic phospholipids; n.a., not available; n.d., not determined

[a] Based on the tissue wet weight.

[b] Fractional tissue volume of intracellular water of Rodgers et al. (2005) reduced by new lysosomal compartment.

[c] Calculated by subtracting the fractional volume of extracellular water of the liver from total tissue Volume and subsequently multiplying by the previously determined fractional volume of lysosomes in hepatocytes (Schmitt et al., 2019). Fractional volumes of tissues were scaled from liver by their BMP content.

[d] Rodgers et al. (2005)

[e] Rodgers and Rowland (2007)

DMD Fast Forward. Published on November 4, 2020 as DOI: 10.1124/dmd.120.000161
This article has not been copyedited and formatted. The final version may differ from this version.

Table 2: Concentration of BMP in rat tissues with corresponding fractional volumes of lysosomes. Liver was taken as reference, whose lysosomal content was determined experimentally. Other tissues were calculated relatively to the liver by bis(monoacylglycero)phosphate (BMP) tissue concentrations.

Tissue	BMP concentration [a] [pmol/mg Tissue]	Fractional tissue volume of lysosomes
Blood cells	< LLOQ	-
Plasma	< LLOQ	-
Adipose	0.3 ± 0.1	0.03 %
Brain	15 ± 1.9	1.4 %
Gut[b]	14 ± 6.8	1.2 %
Heart	3.5 ± 0.6	0.32 %
Intestine	15 ± 6.0	1.4 %
Intestine large	9.6 ± 1.9	0.88 %
Kidney	19 ± 2.6	1.7 %
Liver	14 ± 3.5	1.3 %
Lung	17 ± 5.7	1.5 %
Muscle	1.2 ± 0.1	0.11 %
Skin	1.8 ± 0.6	0.16 %
Spleen	58 ± 4.8	5.3 %
Stomach	12 ± 1.9	1.1 %

[a] Taken from Wang & Schmitt et al. (2019), Data represents mean ± SD

[b] Gut represents the weighted mean of small and large intestine accounting for the 2.3x higher volume of the small intestine

DMD Fast Forward. Published on November 4, 2020 as DOI: 10.1124/dmd.120.000161
This article has not been copyedited and formatted. The final version may differ from this version.

Table 3: Fold increase in predicted Kpu of 27 basic lipophilic drugs in rat tissues by incorporating lysosomal trapping into the mechanistic model compared to Rodgers et al. (2005) (Eq. 2 versus Eq. 3)

Tissue	Fold increase of Kpu min – max (mean)
Adipose	1.00 – 1.08 (1.01)
Brain	1.01 – 1.81 (1.31)
Gut	1.00 – 1.72 (1.11)
Heart	1.00 – 1.20 (1.03)
Kidney	1.00 – 2.09 (1.11)
Liver	1.00 – 1.74 (1.08)
Lung	1.00 – 1.94 (1.11)
Muscle	1.00 – 1.06 (1.01)
Skin	1.00 – 1.11 (1.02)
Spleen	1.01 – 4.09 (1.43)

DMD Fast Forward. Published on November 4, 2020 as DOI: 10.1124/dmd.120.000161
This article has not been copyedited and formatted. The final version may differ from this version.

Table 4: Compound specific parameters, *in vivo* PK and predicted Vuss of 13 protein kinase inhibitors. Physicochemical parameters were predicted using ADMET Predictor™ (Simulations Plus Inc.). Unbound fraction in plasma and blood to plasma concentration ratios were measured experimentally. *In vivo* Vss was obtained from literature or *in vivo* PK studies. The amount of intracellular drug located in lysosomes (% in lysosomes) was calculated according to eq 1.

Compound	pK_a	LogP	*fu*[a]	B:P[a]	Vss exp. [L/kg][c]	Vuss exp. [L/kg][d]	Vuss pred. [L/kg][b]	% in lysosomes
Afatinib	8.4, 3.9	3.8	0.11	2.6	16	152	224	54
Bosutinib	8.4, 4.1	4.1	0.09	1.1	15	177	93	51
Cediranib	9.1, 3.4	4.1	0.14	1.6	5.5	41	90	54
Crizotinib	9.7, 4.1	3.6	0.04	0.94	2.9	82	130	57
Dasatinib	6.9, 3.9	4.0	0.05	1.1	6.3	140	245	31
Gefitinib	6.9, 4.1	3.8	0.04	0.8	9.2	259	142	31
Imatinib	8.2, 4.5	4.4	0.02	0.86	2.6	165	288	60
Lapatinib	6.5, 4.1	4.6	0.003	0.48	1.8	551	1085	20
Masitinib	8.1, 4.2	5.0	0.03	0.83	6.2	236	411	55
Saracatinib	8.1, 5.0	3.2	0.10	1.7	10	97	130	69
Sunitinib	9.0	2.9	0.03	1.6	5.5	171	375	53
Tandutinib	8.9, 4.6	4.3	0.37	2.8	47	127	76	62
Vandetanib	8.8, 4.2	4.5	0.14	2.3	27	189	157	57

[a] Sources: Bosutinib, FDA (2012); Dasatinib, Kamath et al. (2008); Gefitinib, EMA (2008a); Imatinib, O'Brien and Fallah Moghaddam (2013); Lapatinib, O'Brien and Fallah Moghaddam (2013); Sunitinib, EMA (2006)

[b] Detailed prediction results (i.e. Kpu of tissues) are summarised in Table S5.

[c] Sources: Afatinib, EMA (2013); Bosutinib, FDA (2012); Crizotinib, PMDA (2012); Dasatinib, Lombardo et al. (2004); Gefitinib, McKillop et al. (2004); Lapatinib, EMA (2008b);Saracatinib, Hennequin et al. (2006); Sunitinib, EMA (2006); Vandetanib, TGA (2013)

[d] Calculated from experimental volume of distribution and fraction unbound in plasma.

DMD Fast Forward. Published on November 4, 2020 as DOI: 10.1124/dmd.120.000161
This article has not been copyedited and formatted. The final version may differ from this version.

Table 5: Composition of liver Kpu by subcellular distribution processes calculated by eq. 3 for Nicotine and Propranolol-R. ***Abbr.: IW, intracellular water; EW, extracellular water; APL, acidic phospholipids; NL/NPL, neural lipids and phospholipids; Lyso, lysosomes***

Compound	Partial liver Kpu					Liver Kpu
	IW	EW	APL	NL/NPL	Lyso	
Nicotine	1.2	0.2	0.0	0.1	1.1	2.5
Propranolol-R	1.4	0.2	668	0.7	1.5	671

DMD Fast Forward. Published on November 4, 2020 as DOI: 10.1124/dmd.120.000161
This article has not been copyedited and formatted. The final version may differ from this version.

15. Supplements

- ***Supplemental Data***

Fig 1.

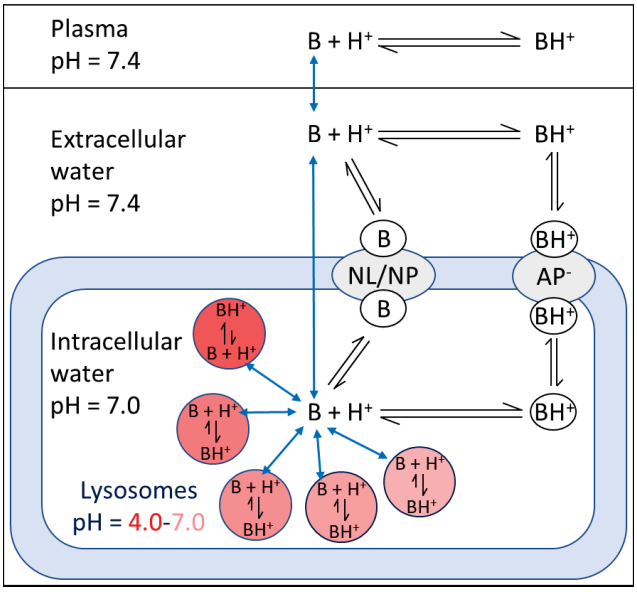

Fig . 2

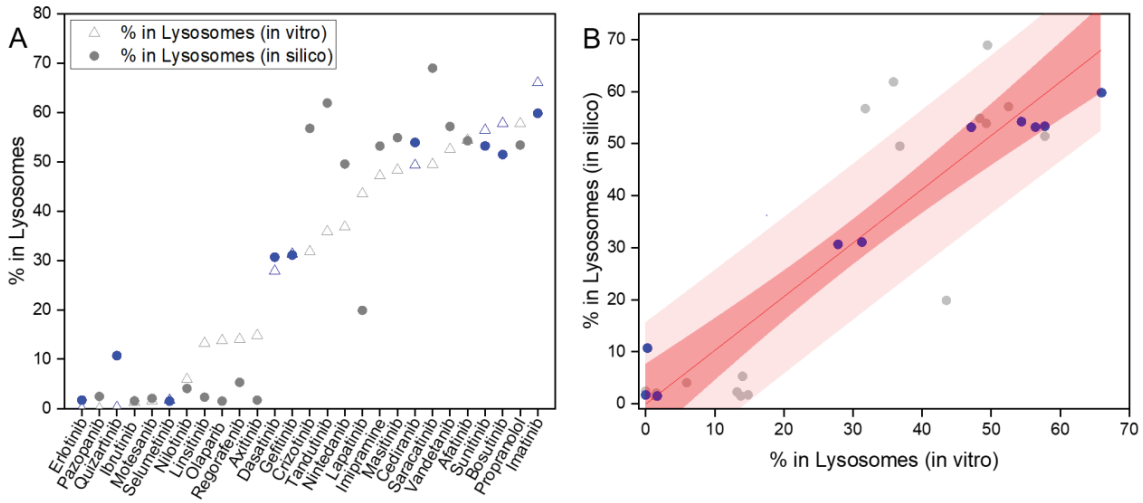

Fig. 3

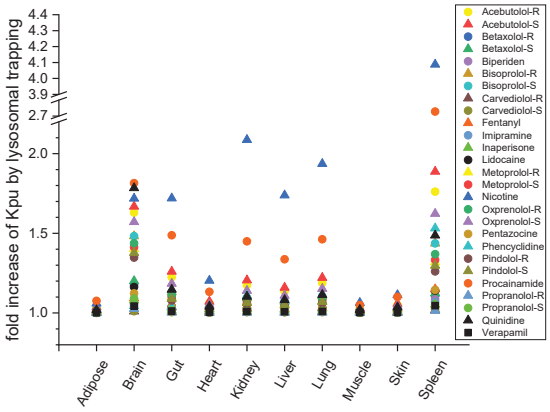

DMD Fast Forward. Published on November 4, 2020 as DOI: 10.1124/dmd.120.000161
This article has not been copyedited and formatted. The final version may differ from this version.

Fig. 4

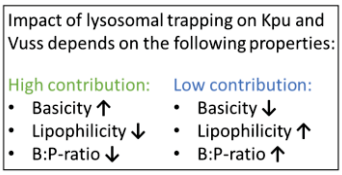

Fig. 5

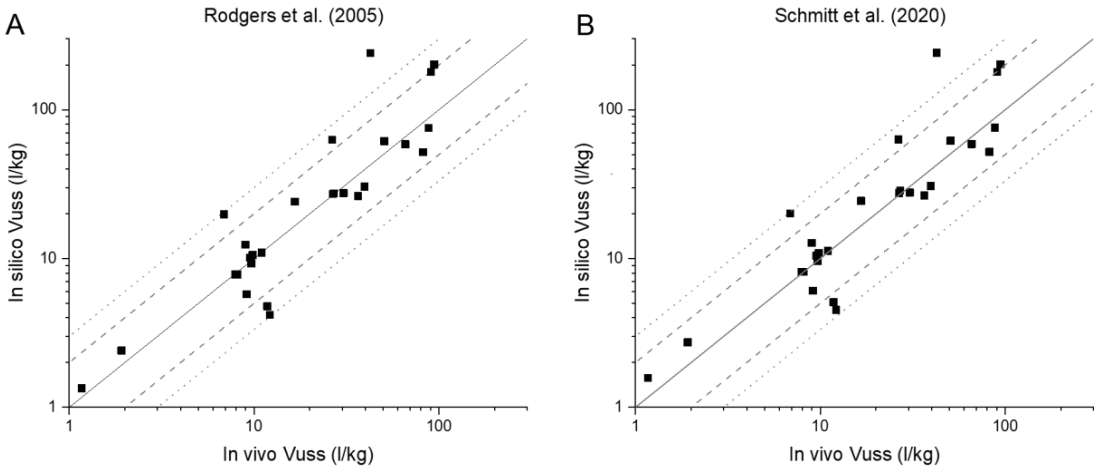

Fig 6.